Invited paper

Dual-mode AlGaInAs/InP square microlasers for terahertz generation

Yue-De Yang, Hai-Zhong Weng, Jin-Long Xiao, and Yong-Zhen Huang *
State Key Laboratory on Integrated Optoelectronics,
Institute of Semiconductors & University of Chinese Academy of Sciences,
Chinese Academy of Sciences, Beijing 100083, China
* Email: yzhuang@semi.ac.cn

(Received 25 September 2017)

Abstract: Dual-transverse-mode AlGaInAs/InP square microlasers with the frequency intervals in the range from several GHz to sub-THz are demonstrated. A sub-THz signal of 103.2 *GHz* is successfully obtained with a uni-traveling-carrier photodiode. For extending the frequency range to THz, deformed square microlasers with the flat sidewalls replaced by circular-arcs are proposed. An increase of mode interval and an enhancement of mode quality factor are realized simultaneously according to numerical simulation results. Furthermore, the stability of dual-mode lasing is verified by a nonlinear gain analysis based on the simulated mode field distributions. For the AlGaInAs/InP deformed square microlasers, beating signals with the frequencies of 0.43, 0.31, and 0.16 *THz* are demonstrated by an autocorrelation measurement, which indicate the microlasers as a novel architecture for the THz wave generation.

Keywords: Dual-mode lasing, Square microlaser, Optical heterodyne, Terahertz wave.

doi: 10.11906/TST.077-086.2017.09.06

1. Introduction

Terahertz (THz) waves, which fall in between infrared light waves and microwaves, have attracted considerable attention because of their potential applications in medical imaging, sensor technology, THz communications, and non-destructive detection [1-4]. Various THz sources based on electronic or optoelectronic devices have been investigated, among which the optoelectronic method is a promising technique. By using the optical heterodyne technique, various dual-wavelength semiconductor lasers operating around 1550 *nm* have been studied for the THz generation, due to their merits of compact structure and low power consumption, [5-13]. Two solitary distributed feedback (DFB) or distributed Bragg reflector (DBR) lasers were firstly used as the sources for optical beating [5, 6]. In order to realize a more compact device with stable wavelength interval, monolithically integrated dual-mode DFB or DBR laser was applied [7-10]. A broad tuning of the frequency interval was realized in an external-cavity laser by changing the grating angles [11]. However, dual-mode DFB or DBR laser requires a precise control of the gratings by a complex electron-beam direct-writing technique [12, 13].

Whispering-gallery modes (WGMs) square microlasers were investigated as potential light sources for on-chip optical interconnection and photonic integrated circuits [14-18]. The robust structure design of the square microlasers permits a high tolerance in fabrication process. Square microresonators with a vertex waveguide can support both the fundamental and the first-order modes with high quality (*Q*)-factor, which results in dual-mode lasing of the square microlasers [16, 17]. Dual-mode lasing with a tunable interval was demonstrated in a 30-μm-side-length square microlaser with a patterned injection window for generating tunable microwave signal [16]. A smaller size device with a higher frequency beating signal at sub-THz is demonstrated using uni-traveling-carrier photodiode (UTC-PD) [17]. Although the transverse mode interval is inversely proportional to the cavity size, dual-mode lasing is difficult to achieve by further reducing the square size because of the low *Q* factor of the first-order mode. Therefore, we propose deformed square microlasers with the flat side replaced by circular arcs to increase the mode interval. For the deformed microsquare AlGaInAs/InP lasers with a side length of 16 μm and a 1.5 μm-wide vertex output waveguide, dual-mode lasing with wavelength intervals of 3.43, 2.46, and 1.26 *nm* is realized by changing the arc radius. The corresponding beating pulses with the repeating frequencies of 0.43, 0.31, and 0.16 *THz* are obtained according to the autocorrelation measurement.

2. Sub-THz signal generation based on dual-mode square microlasers

The square microlasers with a vertex output waveguide are fabricated using an AlGaInAs/InP laser wafer with six pairs of compressively strained multiple-quantum-wells (MQWs) as in [19]. The quantum-well and barrier layers with thicknesses of about 6 *nm* and 9 *nm* are sandwiched between two 90 *nm* AlGaInAs separate-confinement heterostructure (SCH) layers. On top of the upper SCH layer, there are a 1.2 μm-thick p-InP upper confinement layer and a 0.1 μm-thick p^+-InGaAs contacting layer. The square resonator patterns are transferred onto the SiO_2 layer using contacting photolithography and inductively coupled-plasma (ICP) etching techniques, and the laser wafer is etched to about 4.5 μm using ICP technique again with the patterned SiO_2 layer as a hard mask. Figure 1(a) shows the side-view scanning-electron microscope (SEM) image of a square resonator after ICP etching. Figure 1(b) shows the top-view optical microscope image of a fabricated square microlaser. The fabricated microlasers are tested at a temperature of 288 *K* by butt-coupling a tapered single-mode fiber (SMF) to the cleaving facet of the output waveguide.

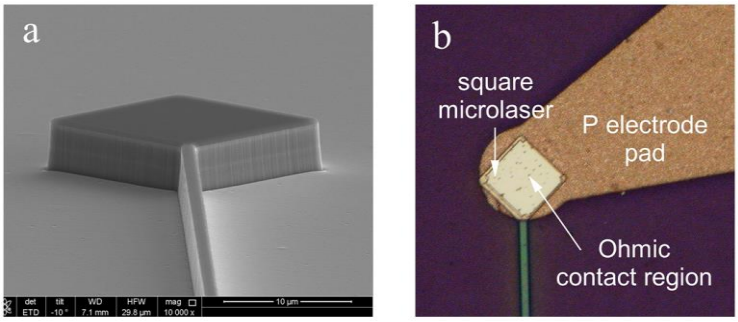

Fig. 1 (a) Side-view SEM images of the waveguide-coupled microsquare resonator after the ICP etching. (b) Optical microscope image of the fabricated microlaser after p-electrode metal deposition.

Figures 2(a) shows the lasing spectrum of a square microlaser with a side length of 20 μm at a continuous injection current of 50 *mA*. Dual-transverse-mode lasing is realized with the peak wavelengths at 1560.03 and 1559.74 *nm*, which corresponds to the fundamental (0th-order) and first-order (1st-order) transverse modes, respectively. The transverse mode interval is 0.29 *nm*, and two weak four-wave-mixing peaks are observed, confirming the coexistence of the two lasing modes. Figure 2(b) shows the experimental setup for detecting the beating signal. The laser output is firstly pre-amplified by an erbium-doped-fiber amplifier (EDFA) and filtered by an optical band-pass-filter (BPF). The filtered spectrum around the main peaks is represented in the inset in Fig. 2(a). Then the filtered optical signal is detected by a 30 *GHz* PD and measured by an electrical spectrum analyzer (ESA). As shown in Fig. 2(c), a main beating signal at 35.9 *GHz* is obtained, corresponding to the frequency interval of the two lasing modes. The inset in Fig. 2(c) shows the normalized spectrum around the peak in a linear scale. Using the Lorentz fitting, a linewidth of about 12 *MHz* is obtained. The microwave linewidth is much smaller than the lasing modes with the linewidths of 102 and 88 *MHz*, which are measured by the optical heterodyne method with a narrow linewidth tunable laser. The results indicate that dual-mode square microlaser can utilized for the microwave signal generation. Dual-mode lasing in one single cavity can have strong mode coherence due to the overlap of mode fields and the synchronous variation of carriers.

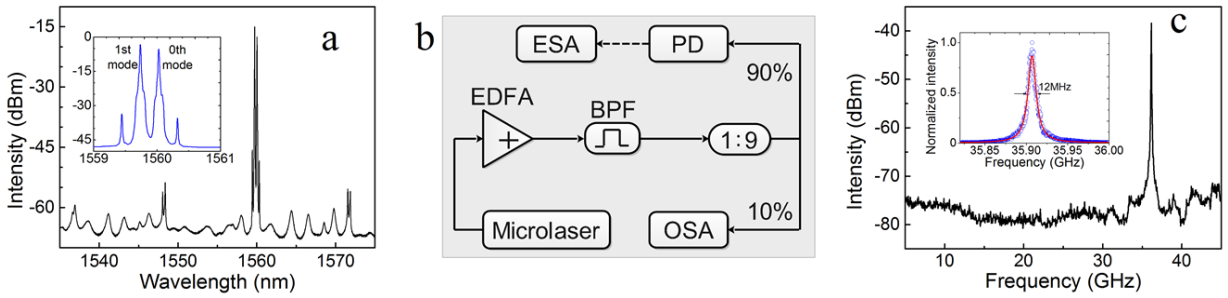

Fig. 2 (a) Lasing spectrum for a square microlaser with a side-length of 20 μm at an injection current 50 *mA*. Inset: zoom in of the spectrum after EDFA and BPF. (b) Experimental setup for microwave generation. EDFA = erbium-doped fiber amplifier; BP = band-pass filter; PD = photodiode; ESA = electrical spectral analyzer; OSA = optical spectral analyzer. (c) Measured beating microwave signal. Inset: Lorentz fit of microwave peak.

Figure 3(a) shows the dual-mode lasing spectrum of a square microlaser with a side-length of 18 μm at 32 *mA*. The lasing wavelengths of the 0th-order and 1st-order mode are 1550.37 and 1549.55 *nm*, respectively. The corresponding transverse mode interval is 0.82 *nm*, i.e., 103 *GHz*. Figure 3(b) shows the schematic illustration of the experimental system for THz signal generation using the dual-mode square microlaser. Differently from Fig. 2(b), a dual-drifting layer based UTC-PD is used to convert the light to electrical signal [20]. In the UTC-PD, the carrier overshoot effect is maintained even under high reverse bias owing to the optimized electric field in the InP carrier drift region, and then a high bandwidth of 102 *GHz* and a high saturation current are achieved simultaneously. The laser output was firstly amplified by an EDFA with a gain of 32 *dB* and filtered by an optical BPF, and then applied to the UTC-PD. The output was fed into an ESA with a Keysight 11970 *W* Harmonic Mixer. Figure 3(c) depicts the observed sub-THz signal, which indicates a center frequency of 103.2 *GHz* with a linewidth of ~110 *MHz* according to the Lorentz fitting. The other signals correspond to the local oscillator induced peaks in the frequency mixer. However, the unpacked laser and UTC-PD chips were coupled with SMFs, and the signal linewidth was broadened due to the system instability and/or signal drifting. We expect that a compact THz source with a high stability can be realized by the integrating microlaser, amplifier and PD on a same chip.

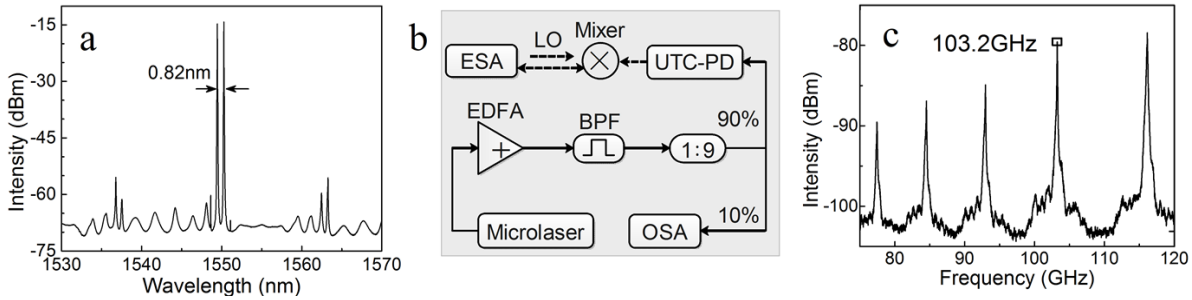

Fig. 3 (a) Lasing spectrum for a square microlaser with a side-length of 18 μm at 32 *mA*. (b) Experimental setup for sub-THz signal generation based the dual-mode square microlaser. LO = local oscillator. (c) Measured sub-THz wave spectrum using the dual-mode spectrum shown in (a) and the setup shown in (b).

3. Dual-mode deformed square microlasers with mode intervals in THz region

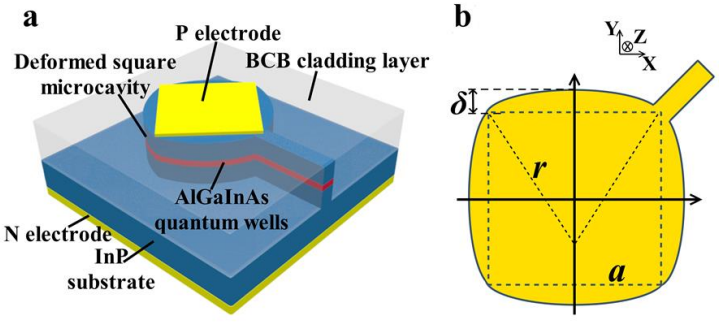

Fig. 4 (a) 3D schematic diagram of a deformed square microlaser with an output waveguide connected to one vertex. (b) 2D schematic diagram of the deformed square microresonator.

In order to extend the frequency interval of the dual-mode microlaser to THz region, we introduce a novel circular-side deformed square resonator, which can modify the lasing characteristics by increasing transverse mode intervals and enhancing mode *Q* factors. The circular-sides can work as concave mirrors for focusing the mode light beam, which is widely used in conventional gas or solid laser systems but rarely used in microresonators with the size comparable to the wavelength. Figure 4(a) shows the three-dimensional (3D) schematic diagram of a deformed square microlaser with the square sides replaced by circular arcs, which is laterally surrounded by a bisbenzo-cyclobutene (BCB) layer and connected to an output waveguide at one vertex. Figure 4(b) shows the two-dimensional (2D) schematic diagram of the deformed square microresonator, the side-length of the square resonator, the width of the waveguide and the curve radius of the arcs are *a*, *w*, and *r*, respectively, where *r* is larger than the circumradius of the square错误!未找到引用源。错误!未找到引用源。. The deformation parameter δ 错误!未找到引用源。错误!未找到引用源。is defined as $\delta = r - \sqrt{r^2 - \boldsymbol{a}^2/4}$.

By solving the wave equation with the finite element method (FEM, COMSOL Multiphysics 5.0), we investigate the influence of the deformation on the mode characteristics numerically [18]. The microresonator with a = 16 μm and w = 1.5 μm is considered and the effective refractive indices of the resonator and surrounded BCB are taken to be 3.2 and 1.54, respectively. Transverse-electric (TE) polarization modes, with the z-direction magnetic field $|H_z|$ satisfying symmetric condition relative to the centerline of the waveguide, are simulated. The mode field distributions $|H_z|$ of the fundamental and the first-order transverse modes are plotted in Figs. 5(a1) and 5(a2) at δ = 0, respectively, while Figs. 5(b1) and 5(b2) shows the corresponding mode field distributions at δ = 1.3 μm. The modes fields of the fundamental and the first-order modes are widely distributed in a square resonator as shown in Fig. 5(a). As a comparison, the mode field patterns have narrow transverse field distributions in the deformed square resonator as shown in Fig. 5(b), which results in ultrahigh mode *Q* factors as the field fields have small radiation loss at the vertices.

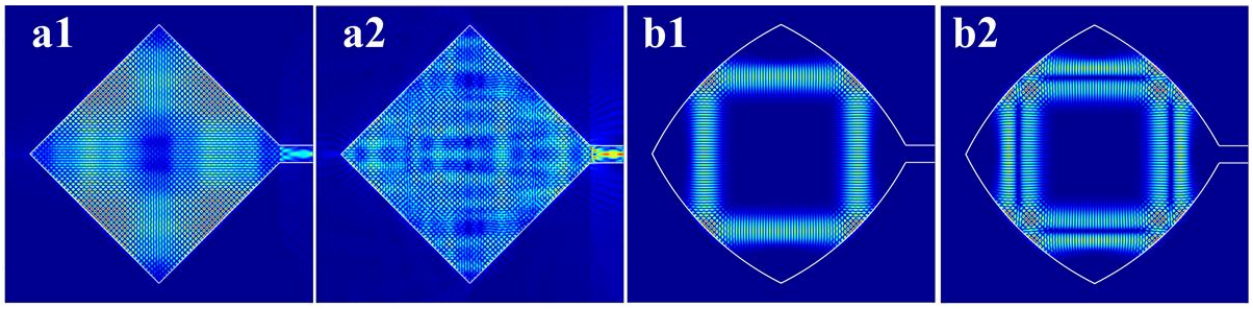

Fig. 5 $|H_z|$ field distributions of (a1) the fundamental and (a2) the first-order modes in the square microresonator with δ = 0, (b1) the fundamental and (b2) the first-order modes in the deformed square microresonator with δ = 1.3 μm. The fields on the right side including the output waveguide are magnified by two times for a clear illustration.

Table 1 summarizes the calculated mode wavelengths and *Q* factors of the fundamental and the

first-order modes as δ = 0, 1.1, 1.3, and 1.5 μm. The wavelength interval of the square microlaser is only 1.04 *nm*, while the intervals are 4.05, 2.69, and 1.48 *nm* for the deformed square microlaser with δ = 1.1, 1.3, and 1.5 μm, respectively. The detailed mode characteristics and wavelength interval variation law can be found in [18]. The *Q* factors of the fundamental and the first-order modes are 1.2×10^4 and 2.3×10^3, respectively, as δ = 0, i.e., for the square resonator without the deformation. The corresponding mode *Q* factors are 1.3×10^{11}, and 2.1×10^{10} as δ = 1.3 μm, which are almost seven orders of magnitude higher than that in the perfect square resonator. The ultra-high passive mode *Q* factors of the fundamental and the first-order transverse modes will result in dual-mode lasing, as they can have near equal mode *Q* factors accounting the internal absorption loss.

Then we demonstrate the stability of dual-mode lasing for square resonator microlasers based on nonlinear gain analysis of density matrix formalism [21]. Accounting the nonlinear gain, the mode gain G_m of mode *m* can be expressed as

$$G_m = g_m - \sum_k G_{m(k)} S_k \tag{1}$$

where g_m is the first-order gain coefficient and S_k is the photon density of mode *k*. The third order gain coefficient $G_m(k)$ is related to the overlap between the intensity of the mode *m* and the spatial distribution of the carrier hole burning caused by the mode *k* as

$$G_{m(k)} = \frac{c}{1+\delta_{m,k}} \int | F_m(r) F_k(r) |^2 \tag{2}$$

where $F_m(r)$ and $F_k(r)$ are the field distributions of modes *m* and *k*, *c* is a constant proportional to the linear gain and relates to the carrier intraband relaxation times, and $1/(1+\delta_{m,k})$ comes from the numbers of field component combinations in squared electric field. Based on dual-mode rate equation analysis, the dual-mode stationary solution is stable if and only if the cross-saturation coefficient is smaller than the self-saturation coefficient, i.e., the ratio of $G_m(k)/G_k(k) < 1 (m \neq k)$ [22].

Tab. 1 Calculated mode wavelength, *Q* factors, and the ratio of cross saturation coefficient to self-saturation coefficient

δ (μm)	0		1.1		1.3		1.5	
Mode	0th	1st	0th	1st	0th	1st	0th	1st
Wavelength (*nm*)	1531.32	1530.28	1555.45	1559.49	1559.55	1562.25	1563.54	1565.03
Q factor	1.2×10^4	2.3×10^3	1.3×10^6	5×10^4	1.3×10^{11}	2.1×10^{10}	1.2×10^{11}	4.9×10^9
$G_{0(1)}/G_{0(0)/1(1)}$	0.95	0.95	0.64	0.83	0.66	0.82	0.82	0.67

In the square resonator, the mode field patterns are determined by the mode numbers *p* and *q*,

which denote the wave node numbers along the directions of the square sides [23]. Both p and q are different between the nearby high Q WGMs, even if they have the same longitudinal mode number or transverse mode number. For example, the fundamental and the first-order transverse modes with the same longitudinal mode number will have the mode numbers of (p, p+2) and (p-1, p+3). So the ratio of the cross-saturation coefficient to the self-saturation coefficient should satisfy the stable condition of dual-mode stationary solution. For the deformed square, the ultra-high Q modes with mode field patterns as shown in Figs. 4(b) are mainly determined by the longitudinal and transverse mode numbers again, instead of the aforementioned mode numbers p and q. We have found that the nearby fundamental and first-order transverse modes belong to different longitudinal mode numbers as $\delta > 0.6\ \mu m$, due to the increase of the transverse mode interval [18]. So they should also satisfy the stable condition for dual-mode lasing. Based on Eq. (2), we calculate $G_m(k)/G_k(k)$ for nearby ultra-high Q modes as δ = 0, 1.1, 1.3 and 1.5 μm and summarize the results in Table 1, where the subscripts "0" and "1" indicate the fundamental and the first-order transverse modes, respectively. The ratios are close to 1 at δ = 0 and far smaller than 1 at δ = 1.1, 1.3 and 1.5 μm. Considering the stable condition for dual-mode lasing and high Q factors, dual-mode lasing can be expected for the deformed square microlasers by choosing a suitable deformation value.

Using the same fabrication process as the square microlasers, we fabricate the deformed square microlasers with side-lengths of 16 μm and δ = 1.1, 1.3 and 1.5 μm. The measured lasing spectra at 31 mA are shown in Figs. 6(a)-6(c) for the microlasers with δ = 1.1, 1.3 and 1.5 μm, respectively. The side-view SEM image after ICP etching is shown in the inset of Fig. 6(a), and the top-view optical microscope image is shown in the inset of Fig. 6(b). The fundamental, the first-order, the second-order, and the third-order transverse modes are assigned by comparing the experimental spectra with the numerical simulation results, and marked by circles, triangles, squares, and pentagrams, respectively. Two main transverse modes lasing simultaneously are clearly observed with the wavelengths of 1553.84, 1552.44, 1555.25 nm for the fundamental transverse modes, and 1557.27, 1554.9, 1556.51 nm for the first-order transverse modes, as δ = 1.1, 1.3, and 1.5 μm, respectively. The corresponding mode intervals $\Delta\lambda$ are 3.43, 2.46, and 1.26 nm, respectively.The intensity ratios between the two lasing modes are 0.5, 0.2, and 0.5 dB, and the intensities of the other peaks are more than 23 dB lower than the main lasing modes. Although super high Q factors are obtained simultaneously for multi-transverse-mode in the simulation, the 2D model does not consider out-of-plane radiation, which may reduce the Q factors of the higher order transverse modes greatly.

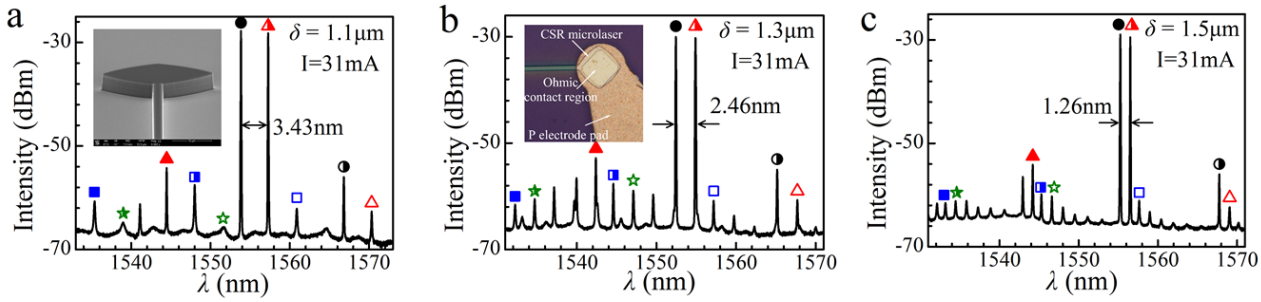

Fig. 6 (a)-(c) Lasing spectra for the deformed square microlasers with a = 16 and w = 1.5 at δ of 1.1, 1.3, and 1.5 μm, respectively. The 0th, 1st, and 2nd, and 3rd order transverse modes are marked by circles, triangles, squares, and pentagrams, respectively, with the open, half-filled, and solid symbols belong to different longitudinal modes. Insets in (a) and (b) are a side-view SEM image after ICP etching and a top-view microscope image of a deformed square microlaser.

Finally, we demonstrate the generation of THz beating pulses based on the deformed square microlasers by the autocorrelation measurement. As is shown in Fig. 7(a), the dual-mode output signal of the deformed square microlaser is pre-amplified by an EDFA. Then the amplified output is filtered by a tunable optical BPF, and split up two parts. 1% of the light is injected to an OSA for monitoring the optical spectra and 99% of the light are further amplified and injected to the auto-correlator to detect the beating signals after the fiber polarization controller (FPC). The autocorrelation pulse trains are measured and plotted in Fig. 7(b) for the deformed square microlasers as δ is 1.1, 1.3, and 1.5 μm, respectively. The emitted pulse trains indicate the uniform sinusoidal modulation, and the average periods are 2.3, 3.2, and 6.4 *ps* as δ = 1.1, 1.3, and 1.5 μm, respectively, which correspond to the repeating frequencies of 0.43, 0.31, and 0.16 *THz*.

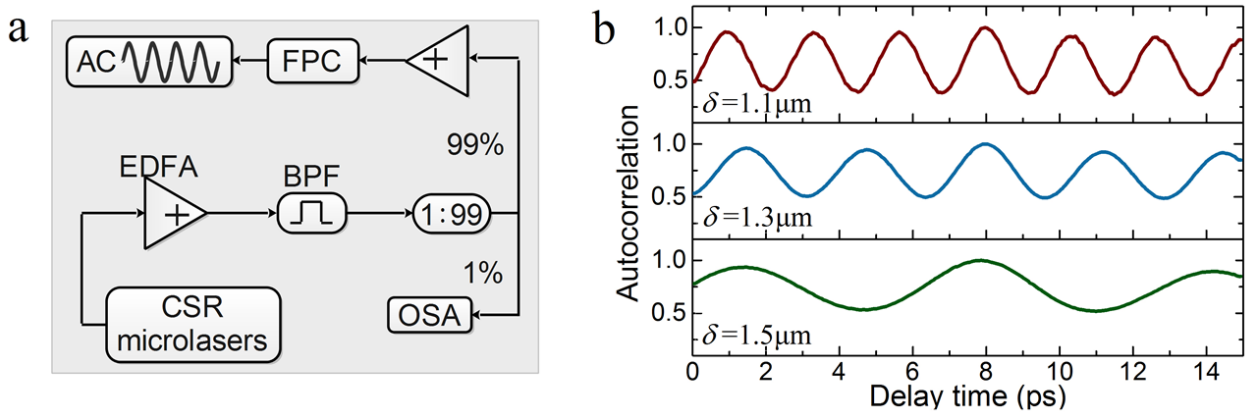

Fig. 7 Autocorrelation measurements based on the dual-mode deformed square microlasers. (a) Experimental setup. (b) Measured autocorrelation pulse trains for the microlasers with δ = 1.1, 1.3 and 1.5 μm, respectively. FPC = fiber polarization controller; AC = autocorrelator.

4. Conclusions

Dual-mode AlGaInAs/InP square and deformed square microlasers have been demonstrated for the generation of sub-THz and THz waves. A 103.2 *GHz* signal is successfully obtained based on the dual-mode square microlaser with the help of high-speed UTC-PD. Deformed square microlasers with circular-side are proposed to realize stable dual-mode lasing and to further extend the mode interval to THz region. The beating pulses with the repeating frequencies up to 0.43 *THz* are demonstrated by an autocorrelation measurement based on the deformed square microlasers. With the advantages of small size and integration compatibility, we expect the dual-mode square and deformed square microlasers can be used as compact THz sources for high-capacity THz wireless communications.

Acknowledgments

The authors would like to thank Osamu Wada of Kobe University, Jin Li, Bing Xiong, Chang-Zheng Sun and Yi Luo of Tsinghua University for the support of THz measurement and valuable discussions

References

[1] M. Tonouchi. Cutting-edge terahertz technology. *Nat. Photonics*, 1, 97-105 (2007),

[2] I. Hosako, N. Sekine, M. Patrashin, et al. “At the dawn of a new era in terahertz technology”. *Proc. IEEE*, 95, 1611-1623 (2007).

[3] T. Kleine-Ostmann, and T. Nagatsuma. “A Review on Terahertz Communications Research”. *J. Infrared Milli.. Terahz Waves*, 32,143-171 (2011).

[4] F. Sizov.THz radiation sensor. *Opto-Electron. Rev.*, 18, 10-36 (2010).

[5] K. A. McIntosh, E. R. Brown, K. B. Nichols, et al. “Terahertz photomixing with diode lasers in low-temperature-grown GaAs”. *Appl. Phys. Lett.*, 67, 3844-3846 (1995).

[6] J. R. Demers, R. T. Logan Jr., and E. R. Brown. “An Optically Integrated Coherent Frequency-Domain THz Spectrometer with Signal-to-Noise Ratio up to 80 dB”. Proceed*ings of the IEEE International Topical Meeting on Microwave Photonics*, Victoria, Canada, 92–95 (2007).

[7] A. Klehr, Jorg Fricke, A. Knauer, et al. “High-Power Monolithic Two-Mode DFB Laser Diodes for the Generation of THz Radiation”. *IEEE J. Sel. Top. Quantum Electron.*, 14, 289-294 (2008).

[8] M. Uemukai, H. Ishida, A. Ito, et al. “Integrated AlGaAs Quantum-Well Ridge-Structure Two-Wavelength Distributed Bragg Reflector Laser for Terahertz Wave Generation”. *J. Appl. Phys*., 51, 0205 (2012).

[9] N. Kim, J. Shin, E. Sim, et al. “Monolithic dual-mode distributed feedback semiconductor laser for tunable continuous-wave terahertz generation”. *Opt. Express*, 17,13851-13859 (2009).

[10] S. Hoffmann, M. Hofmann, M. Kira, et al. "Two-colour diode lasers for generation of THz radiation". *Semicond. Sci. Technol.*, 20, S205 (2005).

[11] S. Pajarola, G. Guekos, and J. Mork. "Optical generation of millimeter-waves using a dual-polarization emission external cavity diode laser". *IEEE Photon. Technol. Lett.*, 8, 157-159 (1996).

[12] F. Pozzi, R. M. De La Rue, and M. Sorel. "Dual-Wavelength InAlGaAs–InP Laterally Coupled Distributed Feedback Laser". *IEEE Photon. Technol. Lett.*, 18, 2563-2565 (2006).

[13] Q. Y. Lu, N. Bandyopadhyay, S. Slivken, et al. "Room temperature single-mode terahertz sources based on intracavity difference-frequency generation in quantum cascade lasers". *Appl. Phys. Lett.*, 99, 131106 (2011).

[14] Y. Z. Huang, K. J. Che, Y. D. Yang, et al. "Directional emission InP/GaInAsP square-resonator microlasers". *Opt. Lett.*, 33, 2170-2172 (2008).

[15] K. J. Che, Y. D. Yang, and Y. Z. Huang. "Multimode resonances in metallically confined square-resonator microlasers". *Appl. Phys. Lett.*, 96, 051104 (2010).

[16] H. Long, Y. Z. Huang, X. W. Ma, et al. "Dual-transverse-mode microsquare lasers with tunable wavelength interval". *Opt. Lett.*, 40, 3548-3551 (2015).

[17] H. Z. Weng, O. Wada, J. Y. Han, et al. "Sub-thz wave generation based on a dual wavelength microsquare laser". *Electron. Lett.*, 53, 939-941 (2017).

[18] H. Z. Weng, Y. Z. Huang, Y. D. Yang, et al. "Mode Q factor and lasing spectrum controls for deformed square resonator microlasers with circular sides". *Phy. Rev. A*, 95, 013883, (2017).

[19] L. X. Zou, Y. Z. Huang, B. W. Liu, et al. "Thermal and high speed modulation characteristics for AlGaInAs/InP microdisk lasers". *Opt. Express*, 23, 2879-2888 (2015).

[20] J. Li, B. Xiong, Y. Luo, et al. "Ultrafast dual-drifting layer uni-traveling carrier photodiode with high saturation current". *Opt. Express*, 24, 8420-8428 (2016).

[21] M. Yamada. "Transverse and longitudinal mode control in semiconductor injection lasers". *IEEE J. Quantum Electron.*, 19, 1365-1380 (1983).

[22] L. Chusseau, F. Philippe, P. Viktorovitch, et al. "Mode Competition in Dual-Mode Quantum Dots Semiconductor Microlaser". *Phys. Rev. A*, 88, 2397-2403 (2013).

[23] W. H. Guo, Y. Z. Huang, Q. Y. Lu, et al. "Modes in square resonators". *IEEE J. Quantum Electron.*, 39, 1563-1566 (2003).